

A hexagonal Fourier model of grid cells

Ulises Rodríguez Domínguez and Jeremy B. Caplan

Department of Psychology and Neuroscience and Mental Health Institute, University of
Alberta, Edmonton, AB, T6G 2E9, Canada

Abstract

Grid cells in rat medial entorhinal cortex are widely thought to play a major role in spatial behaviour. However, the exact computational role of the population of grid cells is not known. Here we provide a descriptive model, which nonetheless considers biologically feasible mechanisms, whereby the grid cells are viewed as a two-dimensional Fourier basis set, in hexagonal coordinates, with restricted availability of basis functions. With known properties imposed into the model parameters, we demonstrate how various empirical benchmark findings are straight-forward to understand in this model. We also explain how complex computations, inherent in a Fourier model, are feasible in the medial entorhinal cortex with simple mechanisms. We further suggest, based on model experiments, that grid cells may support a form of lossy compression of contextual information, enabling its representation in an efficient manner. In sum, this hexagonal Fourier model suggests how the entire population of grid cells may be modelled in a principled way, incorporates biologically feasible mechanisms and provides a potentially powerful interpretation of the relationship between grid-cell activity and contextual information beyond spatial knowledge. This enables various phenomena to be modelled with relatively simple mechanisms, and leads to novel and testable predictions.

Keywords: grid cells; entorhinal cortex; Fourier Transform; context; information compression

A hexagonal Fourier model of grid cells

Introduction

Response characteristics of grid cells in medial entorhinal cortex (MEC) with respect to spatial cognition, and their relationship to hippocampal place cells, have been extensively studied. However, the computational role of grid cells individually and as a population are still under debate. Here we consider how the population of grid cells might be viewed as a set of Fourier basis functions. The idea is compelling because our understanding of the computational roles of grid cells could then benefit from the powerful mathematical properties of the Fourier Transform (FT), but as we elaborate, the analogy to Fourier Transform needs some modification. The idea has been proposed in various forms, that grid cells may function as Fourier components (periodic functions) and whose output at different spatial scales is combined, via synaptic inputs to the place cells, in weighted sums (linear combinations), producing place fields (Solstad, Moser, & Einevoll, 2006; Orchard, Yang, & Ji, 2013; Ormond & McNaughton, 2015). Blair, Welday, and Zhang (2007) hypothesized that MEC grid cells in the dorsal area are Moiré grids formed by the interference of much smaller grids. Oscillatory interference models produce a positional firing rate code based on a phase code at different angles like the 2D model extension for grid cells proposed by Burgess, Barry, and O'Keefe (2007); Burgess (2008). Blair, Gupta, and Zhang (2008) suggested a three-stage oscillatory interference model to convert phase-coded position signals into grid and place cell responses, as rate-coded position signals. Solstad et al. (2006) showed that grid-cell activity can be modelled in the spatial domain as a sum-of-three cosine functions. Later, Orchard et al. (2013) extended this to the frequency domain in polar coordinates, where each cosine function can be viewed as a wave front formed from two-dimensional Fourier basis functions, similarly to each traveling wave at a particular heading angle described by Hasselmo and Brandon (2012) and Hasselmo and Shay (2014). Orchard et al. (2013) further proposed that the connection strengths that project to an individual grid cell constitute individual Fourier coefficients,

which are then mapped to the spatial domain by that grid cell by computing an inverse FT. Since grid cells show a variety of scales and orientations, in accordance with this view (Orchard et al., 2013), it follows that grid cells as a population may comprise a discrete basis set of Fourier functions— which in two dimensions means that such functions, when linearly combined, can reconstruct any two-dimensional discrete function, i.e., spatial pattern. However, some properties of grid cells, such as non-linear sampling of frequencies and a limited number of observed orientations (Stensola et al., 2012) impose constraints on the available set of these Fourier basis functions.

Following Orchard et al. (2013), we present a descriptive model of how the population of grid cells might represent an inverse FT of a discretely sampled signal. Departing from Orchard et al.’s formulation in polar coordinates, our model differs in that it is grounded in Fourier theory on *hexagonal* coordinates. Hexagonal coordinates fit more naturally with the periodic hexagonal place-invariant nature of grid cells observed experimentally (Hafting, Fyhn, Molden, Moser, & Moser, 2005), and naturally incorporate hexagonal sampling, which we explain might be a key property for using fewer grid cells to represent a given signal. We impose known properties of the grid-cell population into the parameters and we consider biophysically plausible mechanisms, approximating a mechanistic account of the model. In particular, we consider how grid cells may deal with complex arithmetic computations in a simple way, based on phase shifts. We show how variations in the model parameter values can result in a variety of phenomena such as grid-field scaling and less regular non-isotropic grid fields, and explain how some redundancy in the Fourier basis functions that compose a grid cell is likely the case. We provide a mathematical proof that an isotropic grid field generated in our hexagonal Fourier model is equivalent to the sum-of-three cosine model of Solstad et al. (2006); thus, our model can be seen as a generalization of that model. Finally, we present model-experiments that suggest the grid-cell system might compute lossy compression of two-dimensional signals with naturalistic stimulus properties.

Methods

Here we describe the inverse Hexagonal Discrete Fourier Transform (HDFT; Mersereau, 1979), then present in detail our proposal of how grid cells could implement such transform. For the grid cell model, we first explain its parameters and what constitutes the grid cell input, and then explain how they relate to known properties of grid cells and the MEC. We then explain how variations in these parameters can give rise to experimentally observed phenomena. A simple mechanism by which grid cells might support complex computations, inherent in a Fourier Transform, is presented next. Finally, in this section we present an interpretation of the computational role of the grid-cell system, namely lossy compression of signals with naturalistic-like properties, in the view of our model.

Inverse Hexagonal Discrete Fourier Transform

The Fourier transform is a mapping from the spatial domain to the frequency domain. Here we deal with 2D signals in both their spatial (\mathbf{x}) and frequency (\mathbf{X}) domain, where we denote variables in the spatial domain with lowercase and in the frequency domain with uppercase letters, and vectors in boldface. Mersereau's HDFT operates over a periodic hexagonal region of support (Figure 1A), with length R from the origin of the hexagon to any of its vertices. R can be seen as the radius of the circle that encloses this region. We denote the horizontal axis of this region at 0° as \mathbf{h}_1 and the “vertical” axis at 120° as \mathbf{h}_2 . The hexagonal region has periodic boundary conditions, just as in the standard rectangular 2D Fourier Transform. The region of support (Figure 1A) is effectively the area outlined by the blue perimeter. We focus on the *inverse* HDFT, the mapping from the frequency domain to the spatial domain, since (e.g., Orchard et al., 2013), this is the operation that grid cells seem to compute. The inverse HDFT, x_{r_1, r_2} , at the two-dimensional spatial point (r_1, r_2) of \mathbf{X} , is (Mersereau, 1979):

$$x_{r_1, r_2} = \frac{1}{3R^2} \sum_{k_1, k_2 \in \Omega_f} X_{k_1, k_2} e^{u+v}, \quad \forall r_1, r_2 \in \Omega_s, \quad (1)$$

over the hexagonal region of support in the frequency domain, Ω_f , where Ω_s denotes the spatial domain, and

$$u = \frac{i\pi (2k_1 - k_2) (2r_1 - r_2)}{3R}, \quad v = \frac{i\pi k_2 r_2}{R}. \quad (2)$$

The u and v terms differ from the standard DFT due to the hexagonal coordinates. It can be appreciated in the u term that the hexagonal coordinates are linearly dependent. This makes the design of fast algorithms more complicated, but Mersereau (1979) provided an algorithm we used for our simulations (code publicly available at <https://github.com/ulisesrdom/GGRIDCELL>).

Slightly departing from Mersereau (1979), we shift the origin to the center of the hexagonal region of support, defining the spatial domain, $\Omega_s = \{(r_1, r_2) \mid 0 \leq r_1 < 2R \text{ and } -R \leq r_2 < R \text{ and } -R \leq r_1 - r_2 < R\}$. The frequency domain, Ω_f , is defined similarly, i.e., switching r_1 and r_2 with k_1 and k_2 , respectively, in the definition of Ω_s .

Each point in hexagonal coordinates corresponds to exactly one point in rectangular coordinates. To map from rectangular to hexagonal coordinates, similarly to Snyder, Qi, and Sander (1999), but changing the contribution of n_2 onto r_1 from negative to positive due to the orientation of the hexagonal axes we use:

$$r_1 = n_1 + \frac{n_2}{\sqrt{3}}, \quad r_2 = \frac{2}{\sqrt{3}}n_2, \quad (3)$$

where n_1 and n_2 correspond to the horizontal and vertical rectangular coordinates, respectively. Since n_1 and n_2 span the real plane \mathbb{R}^2 and each pair (n_1, n_2) has a unique correspondence with a pair (r_1, r_2) , then r_1 and r_2 also span \mathbb{R}^2 ; for a proof, see (Snyder et

al., 1999), but changing the sign from negative to positive in the contribution of n_2 onto r_1 . This implies that points in the hexagonal frequency domain can be used similarly to points in the rectangular frequency domain to build any two-dimensional function in the discrete spatial domain by using an inverse HDFT. Each point in the hexagonal frequency domain can be seen as a Kronecker delta function—a function with value equal to one at that particular frequency point and zero everywhere else—with some scale value (amplitude) that indicates the amount that such particular frequency is present in the two-dimensional spatial signal. The entirety of these scaled Kronecker delta functions in the frequency domain form a complete Fourier basis set to build any two-dimensional discrete function.

Grid cell model

We do not, here, consider the temporal dynamics of grid cells, but rather model the average firing rate of each grid cell as an inverse hexagonal Fourier transform of six frequency components. However, in the future, our model could be extended to simulate temporal dynamics, for which at least oscillatory frequency or firing rate due to running speed as found by Jeewajee, Barry, O’Keefe, and Burgess (2008); Hinman, Brandon, Climer, Chapman, and Hasselmo (2016) would likely play a role in the model parameters. The average firing rate of each grid cell at point $(r_1, r_2) \in \Omega_s$ is:

$$x_{r_1, r_2} = \frac{1}{3R^2} \sum_{j=1}^6 X_{k_1^{(j,\theta)}, k_2^{(j,\theta)}} e^{i(u^{(j,\theta)} + v^{(j,\theta)})}, \quad (4)$$

where

$$u^{(j,\theta)} = \frac{\pi (2k_1^{(j,\theta)} - k_2^{(j,\theta)}) (2r_1 - r_2)}{3R}, \quad v^{(j,\theta)} = \frac{\pi k_2^{(j,\theta)} r_2}{R}, \quad (5)$$

and

$$X_{k_1^{(j,\theta)}, k_2^{(j,\theta)}} =$$

$$A_{k_1, k_2} e^{-\frac{i\pi}{R} \left(\frac{4}{3}(\alpha - \frac{1}{2}\beta) \left(k_1^{(j,\theta)} - \frac{1}{2}k_2^{(j,\theta)} \right) + \beta k_2^{(j,\theta)} \right)}. \quad (6)$$

The parameters for equations 4–6 are as follow:

$\underline{\theta}$: Grid cells have a discrete organization into grid modules in MEC, where up to ten grid modules, each with a single orientation, θ , are estimated to exist in the rat MEC (Stensola et al., 2012). Border cells (Barry et al., 2006; Solstad, Boccara, Kropff, Moser, & Moser, 2008; Lever, Burton, Jeewajee, O’Keefe, & Burgess, 2009; Krupic, Bauza, Burton, & O’Keefe, 2016) in MEC are active when the rat is at the boundary of an enclosure. Along with evidence that grid cells can show different orientations in a single environment if there are distorted boundaries (Krupic, Bauza, Burton, Barry, & O’Keefe, 2015), this suggests boundary cells may orient grid cells. Later we explain how orientation might affect each frequency coordinate differently. Theta cells vary as the cosine of a rat’s allocentric movement direction (Welday, Schlifer, Bloom, Zhang, & Blair, 2011), possibly helping orient grid cells as well. Further, conjunctive grid \times head direction cells already show oriented grid cell responses but only when the head of the rat faces particular orientations (Sargolini et al., 2006). We suggest θ is incorporated in grid cells through previously oriented grid \times head direction cell responses, incorporated at various head orientations and which in turn might depend on both border cells and theta cells. We do not model explicitly how boundary cells and theta cells incorporate θ into grid \times head direction cells, but rather, rotate each frequency point (k_1^j, k_2^j) corresponding to a grid cell according to a rotation matrix in hexagonal coordinates:

$$\begin{bmatrix} k_1^{(j,\theta)} & k_2^{(j,\theta)} \end{bmatrix} = \begin{bmatrix} k_1^{(j)} & k_2^{(j)} \end{bmatrix} \mathbf{Q}_{\text{hex},\theta}, \quad (7)$$

where $\begin{bmatrix} k_1^{(j,\theta)} & k_2^{(j,\theta)} \end{bmatrix}$ denotes the rotation of $\begin{pmatrix} k_1^{(j)}, k_2^{(j)} \end{pmatrix}$ in vector notation and $\mathbf{Q}_{\text{hex},\theta}$ is a rotation matrix in hexagonal coordinates at (counterclockwise) angle θ , defined:

$$\mathbf{Q}_{\text{hex}\theta} = \begin{bmatrix} \cos(\theta) + \frac{\sin(\theta)}{\sqrt{3}} & \frac{2\sin(\theta)}{\sqrt{3}} \\ -\frac{2\sin(\theta)}{\sqrt{3}} & \cos(\theta) - \frac{\sin(\theta)}{\sqrt{3}} \end{bmatrix}. \quad (8)$$

A_{k_1, k_2} : The amplitude A_{k_1, k_2} , an input to the grid cell, represents how much of the 2D spatial frequency at point (k_1, k_2) is present in the signal or combination of signals being transmitted to the MEC, coding a frequency-domain representation. We hypothesize that grid cells have at least six such amplitude inputs at selected points (described later). If A_{k_1, k_2} is the highest amplitude of the frequencies of the grid cell, it also represents the maximum firing rate (no units) a grid cell may have at a particular context in an environment, i.e., the highest responses out of the peaks of a grid field. Pérez-Escobar, Kornienko, Latuske, Kohler, and Allen (2016) showed that the firing rates of 50% of the neurons they recorded in the MEC discriminate different nonmetric visual landmarks in an otherwise unchanged environment, providing evidence that our hypothesized frequency amplitude inputs are affected by visual stimuli. We suggest that the firing rate of each grid cell does not represent this directly, but a sum of these frequency amplitude inputs, weighted by complex exponentials—an inverse FT.

R : The region of support coded by the grid cell in a given environment has a size R , which must be estimated. We suggest R depends on hypothesized cells that signal a distance measure to a prominent visual landmark in the environment, and that border cells may help in estimating this distance measure. The context may change for the rat even within the same environment by moving to a different sub-area with distinct prominent landmarks.

(α, β) : The 2D phase parameter (α, β) sets the location of each peak in a grid field, relative to a reference location. The phase (α, β) of neighbouring grid cells differs (Hafting et al., 2005), even within grid modules (Stensola et al., 2012), so this is the parameter that varies the most across grid cells. In addition, the statistics captured by phase information contain the majority of the information used to discriminate natural scenes (McCotter,

Gosselin, Sowden, & Schyns, 2005). Hence it is feasible for a great variety of features from natural scenes in the environment to be represented in the MEC.

We suggest that environmental features perceived by the rat are represented in a distributed way through the frequency domain amplitudes A_{k_1, k_2} , each multiplied by a certain phase shift (see equation 6). A phase shift is just a multiplication by a cosine on the real part of the signal, and multiplication by that same cosine shifted by $\pi/2$ radians on the imaginary part. Hence, this input might already be represented in the frequency domain once in MEC (Kato & Caplan, 2017, and see Caplan, 2011).

$\{(k_1^{(j,\theta)}, k_2^{(j,\theta)})\}_{j=1}^6$: These frequency coordinate points set the scale for each peak in a grid field in the spatial domain. The frequency (inverse of scale) progression between grid modules in MEC was found to be approximately $\sqrt{2}$ as modules go from ventral to dorsal MEC (Stensola et al., 2012). We suggest grid cells receive at least six such frequency-domain inputs at particular frequency points with the same scale and separated by roughly 60° , but this angular separation might change depending on boundary cell signals, which accounts for distorted patterns when there are distorted boundaries in the environment. If we assume grid cells can only show perfectly hexagonal patterns, then only three of those points are needed. However, three of those frequency inputs do not capture the deformations shown in experimentally recorded grid fields. We think it is likely that each of those fundamental frequency inputs has other redundant inputs, for robustness to noise and to delayed input signals. The least amount of redundancy is to have each fundamental frequency repeated twice, hence we consider six instead of three frequency points. Figure 3 illustrates how six, instead of three, frequency inputs resembles more real grid fields when the input is noisy.

The following is an example of such frequency coordinate points at 0° , with exactly 60° separation between them and isotropic frequency ω :

$$(k_1^{(1,0)}, k_2^{(1,0)}) = (\omega, 0), \quad (k_1^{(2,0)}, k_2^{(2,0)}) = (\omega, \omega),$$

$$\begin{aligned} (k_1^{(3,0)}, k_2^{(3,0)}) &= (0, \omega), \quad (k_1^{(4,0)}, k_2^{(4,0)}) = (-\omega, 0), \\ (k_1^{(5,0)}, k_2^{(5,0)}) &= (-\omega, -\omega), \quad (k_1^{(6,0)}, k_2^{(6,0)}) = (0, -\omega). \end{aligned} \quad (9)$$

Complex computations. If we focus on only one of the six terms in the summation on the right-hand side of equation 4, fixing j , by applying equation 6 and further assuming that θ is fixed, and using $\sin(x) = \cos(x - \pi/2)$, we arrive at the following equation (more detail in Supplementary Materials):

$$\begin{aligned} X_{k_1, k_2} e^{i(u+v)} &= \\ \operatorname{Re} \left[A_{k_1, k_2} \left[\cos(q) \cos(u+v) + \cos\left(q - \frac{\pi}{2}\right) \cos\left(u+v - \frac{\pi}{2}\right) \right] \right] + \\ \operatorname{Im} \left[A_{k_1, k_2} \left[-\cos\left(q - \frac{\pi}{2}\right) \cos(u+v) + \cos(q) \cos\left(u+v - \frac{\pi}{2}\right) \right] \right], \end{aligned} \quad (10)$$

where $\operatorname{Re}[\cdot]$ and $\operatorname{Im}[\cdot]$ denote the real and imaginary parts respectively, u and v are defined as in equation 5, and

$$q = \frac{\pi}{R} \left(\frac{4}{3} \left(\alpha - \frac{1}{2} \beta \right) \left(k_1 - \frac{1}{2} k_2 \right) + \beta k_2 \right). \quad (11)$$

In equation 10 we can see the hypothesized inputs for each term in a grid cell computation. Highlighted in green are the cosines which serve as basis functions to represent the frequency domain signal in the spatial domain. Highlighted in blue are cosines that, together with the amplitude value A_{k_1, k_2} , carry the phase and amplitude information, respectively, of the signal being represented in MEC. Grid \times head direction cells may be good candidates for the cosine basis functions (green cosines), since they also unfold over 2D space but form 1D periodic patterns. On the other hand, phase and frequency information may be carried by hypothesized cells whose firing strength depends on both A_{k_1, k_2} and a corresponding phase shift, naturally included in the stimuli or combination of stimuli being coded in MEC. Because the spatial-domain signal was presumably real-valued, the imaginary part in the right-hand side of equation 10 is zero (Brigham,

1988) or approximately zero due to the presence of noise. For the remaining real part, the input consists of two frequency cells coding a real and an imaginary value, each corresponding to a cosine in blue times A_{k_1, k_2} in equation 10, and another two basis cosine cells coding a real and an imaginary value (grid \times head direction cells), each corresponding to a cosine in green. The only difference between each real-imaginary pair of frequency cells is that they have a phase difference of $\pi/2$, and this is also the case between the real-imaginary pair of basis cosine cells. Further, only excitatory connections are needed to output the real part. Thus, we suggest that complex-valued computations can be carried out in the MEC with such simple mechanisms.

Lossy compression

In signal processing, lossy compression refers to a compression algorithm that loses information from the original signal in the process, with the advantage that it yields a much higher compression ratio than that of lossless compression (Li & Drew, 2004). We suggest grid cells with frequencies sampled with an exponential $\sqrt{2}$ sampling factor and a single orientation in each frequency band within the 60° range (Stensola et al., 2012), could be viewed as efficient filters that implement lossy compression of both spatial and contextual input. In this view, each grid module corresponds to grid cells with a single scale and orientation (a single 2D frequency point) with some variability in both scale and orientation and with many phases.

Blair et al. (2007) hypothesized that a similar mechanism to grid cells in the visual pathway may be involved with storing scale-invariant memories of images, showing that grid fields can serve as a basis set for constructing complex images. Here we not only use grid fields as basis functions but also show that using a very limited subset of such basis functions compatible with experimental findings (Stensola et al., 2012) yields a very efficient compression in naturalistic images, which preserves important information.

To assess the hypothesis that grid cells compute lossy compression of contextual

stimuli, we compared filtering results making sure the same number of grid cells were used in our hexagonal Fourier model in two scenarios: using linear sampling (LS) and using exponential sampling (ES). We tested this with 100 images from a publicly available database by Oliva and Torralba (2001) of 256×256 pixel images in jpeg format. We selected 50 images from the forest data set and 50 images from the open country data set. Images were transformed to grayscale, hexagonally sampled and then the HDFT was applied. In the hexagonal frequency domain, the ES filter was first applied with a specific exponential base and isotropic spread around each 2D frequency point. We selected four orientations in groups of two orientations, each very close (separated by 5°), across grid modules, approximating Stensola et al. (2012), where only two clear peaks were found. A DC frequency component was considered, which might consist of a single neuron, out of the full population of MEC neurons, that computes the average of the signal amplitude values. To quantify similarity, the mean correlation was computed between the original hexagonally sampled images and the filtered images. The same approach was taken with the LS filter, sampling frequency linearly.

Results

Grid cell model. Figure 2 shows examples of different grid fields with their corresponding frequency components, produced using equation 4 (which is the non-reduced form for generating a general grid field). In the second and third row of Figure 2, two grid fields with the same scale and orientation are shown, with zero and non-zero phase, respectively (applied with equation 6). The fourth row of Figure 2 shows an example of grid scale change in one direction, consistent with compressing the room along that direction. Irregular grid fields were produced by adding a small amount of Gaussian noise to the coordinates of the frequency components in each model grid cell, better resembling real grid fields (Figure 3), when using six instead of only three frequency components. This is in line with our suggestion that grid cells receive redundant frequency inputs. In the

supplementary materials, we illustrate place field remapping as conceived by Hayman and Jeffery (2008) but seen from the Fourier domain perspective.

Lossy compression and exponential frequency sampling of stimuli.

Figure 4 shows an example image treated as the visual contextual input, and the result of compression, that is, a kind of down-sampling, by applying two filters: ES and LS. For all of the cases tested (for each base), filtering with exponential frequency sampling yields higher similarity (mean correlation) with the original natural image (Figure 5A). This occurs due to less distortion of the filtered image with respect to the original image. In particular, when the base of the ES filter is $\sqrt{2}$, the obtained mean correlation is the highest among the bases we considered. In Figure 4, hexagonal artifacts can also be seen more when using the LS than when using the ES filter.

Since the power spectrum of natural images is autocorrelated (Field, 1987), also called coloured noise, where power drops with increasing frequency, we repeated the filtering simulations with 10 uniform white noise (equal power at all frequencies) images in grayscale for the same variety of exponential bases and bandwidths. Unlike with natural images, Figure 5B shows that the filters all perform similarly. Similarity is lower in all cases compared to natural images (Figure 5A). This suggests the grid-cell system, and in particular, exponential frequency-sampling, may be optimized for the statistical properties of naturalistic stimuli.

Comparison with the Solstad et al. (2006) model. A popular approach to modelling grid fields is with the sum-of-three cosine waves, 60° apart, introduced by Solstad et al. (2006). In the supplementary material, we show that this model is a special case within the hexagonal Fourier model. We present a proof that equation 4 is functionally the same as the sum-of-three two-dimensional cosine functions proposed by Solstad et al. (2006) in the case of an isotropic grid field.

Discussion

We proposed a descriptive model for the activity of the grid cell population, grounded on Fourier theory adapted to hexagonal coordinates. We explicitly relate our model parameters to either known properties experimentally found in the MEC or with biologically feasible mechanisms and inputs, bringing the model close to a mechanistic account, although we stop short of explicitly considering simulation of neuronal mechanisms for the generation of grid cell activity. Grid cells compute an inverse Fourier transform of environmental features, taking as input a frequency-domain representation in the MEC of the current context where a rat is located.

An advantage of hexagonal coordinates is that they naturally fit with hexagonal sampling, which is known to require 13.4% fewer samples than rectangular sampling for signals band-limited over a circular region of the frequency plane (Mersereau, 1979) and is, in this way, optimal. They also resemble the periodic hexagonal nature of grid fields. Hexagonal sampling suggests the grid cell system may be optimized to sample the explored space efficiently while minimizing the number of cells required.

For a single grid cell, our model has the parameters of orientation, amplitude, size of the region of support, phase and frequency coordinates, which can all be manipulated directly in the frequency domain and compared to the results in the spatial domain (see Figures 2, 3 and 4). This comparison between grid cell's input in the frequency domain and their output in the spatial domain is also useful for understanding place field remapping, as we exemplified in the supplementary materials.

We argued that orientation might be incorporated through grid \times head directions cells at various orientations, in turn depending on border and theta cells. Border cells might affect the orientation of each frequency coordinate parameter differently depending on the boundaries in the environment. The size of the environment represented in MEC is reflected in the size of the region of support, which might be driven by prominent visual landmarks. This could explain why a single grid cell can show different periodic patterns

within a continuous two-dimensional space as observed by Krupic et al. (2015), while still using a Fourier mechanism to account for these distortions, in contrast to Stachenfeld, Botvinick, and Gershman (2017).

Only three fundamental frequency coordinates are needed to generate perfectly hexagonal isotropic grid fields. However, redundancy in those fundamental frequency coordinates is likely the case within a grid cell for more robustness to noise or errors in the input signals. With the minimum amount of redundancy for each fundamental frequency coordinate, six such coordinates, better resembled experimentally observed grid fields in the presence of noise (Figure3). We showed that using only three frequency coordinates separated by sixty degrees is a particular case within our model and actually corresponds to the popular sum-of-three cosine model (Solstad et al., 2006). To our knowledge, this is the first proof of this equivalence. Moreover, this shows that our model is not divergent from prior grid-cell models, but rather, an extension of them.

In our view, environmental features reflecting the actual context of the rat are represented in a distributed way in MEC in the frequency domain in hypothesized frequency cells, which carry information about the phase and frequency-domain amplitude of such features, serving as input to the grid cells.

At the population level, each horizontal band of grid cells in MEC that spans the mediolateral axis at a fixed dorsoventral level is roughly seen as a certain frequency band. Such frequency band has non-zero values concentrated only around six frequency coordinates that span a great variety of phases. This corresponds to a single grid orientation and a geometric increase in frequency as the dorsoventral level changes from ventral to dorsal for each grid module as found by Stensola et al. (2012). This suggests that each grid module may serve the computational role of filtering either 2D signals or the 2D projection of higher-dimensional signals. This is somewhat similar to work by Howard et al. (2014), who provide a framework in which intermediate representations of the physical world regarding either time or space, coded by a set of cells in the hippocampus,

are assumed to be represented in the form of a Laplace Transform, which can be inverted through a set of connections, yielding a reconstruction that approximates the original physical-world signal—a different set of basis functions. We specify what the computational role of the whole grid cell population might be, which not only includes a representation of physical-world signals, but also a lossy reconstruction.

In this view, our computational experiments showed that grid modules acting as filter, when using exponential frequency sampling, preserve natural images better after inverse Fourier transforming compared to linear frequency sampling if the exponential base is kept reasonably small. Specifically out of five tested exponential bases, higher similarity to the original image was obtained when using a $\sqrt{2}$ exponential base but no such advantage for exponential sampling for white noise images. This filtering effect implies a compression of information, thus requiring fewer processing units (grid cells), while minimizing loss of meaningful information, analogous to lossy compression. Regarding the role of the geometric increase in frequency, Stemmler, Mathis, and Herz (2015) showed how grid cell population activity across its different consecutive scales can be decoded for the purpose of self localization and goal-directed navigation. They obtain a scale ratio between grid modules of around 1.5 to minimize the risk of large-scale spatial localization errors. Wei, Prentice, and Balasubramanian (2015) proposed that the grid cell system minimizes the number of neurons required to encode a location at some resolution, obtaining an optimal idealized ratio of square root of e that lies in the range [1.4, 1.7] for realistic neurons. Both arguments for explaining the observed ratio rely on spatial information. Here we have made the argument that the geometric grid progression might also be tuned that way in order to preserve the most important information in natural stimuli signals while representing them in a very compressed way. Like Wei et al. (2015), our argument is also one of requiring fewer neurons, but for representing a signal with naturalistic-like statistical information, i.e., spatially correlated, instead of a particular location. However, both location and fidelity of representation of naturalistic-like signals could play a role in

the observed grid scale ratio, perhaps optimized on a combination of both criteria to minimize the number of grid cells required. This view also raises the possibility that the population of grid cells may perform the same kind of computational role beyond spatial information processing. This is supported by recent evidence that non-spatial contextual stimuli also modify grid-cell activity (Marozzi, Ginzberg, Alenda, & Jeffery, 2015; Pérez-Escobar et al., 2016). As suggested by Pérez-Escobar et al. (2016) and Marozzi et al. (2015), input to grid cells is not only spatial, since visual stimuli affect the phases, and to some degree the firing rate, of grid cells, and olfactory stimuli affect the phases. We hypothesize that more general non-spatial contextual information may also serve as input to the grid cells, possibly as a step in episodic memory formation (Caplan, 2011).

To conclude, grid cells may be viewed as comprising a reduced two-dimensional set of Fourier basis functions, in hexagonal coordinates, with exponential frequency sampling, and with possible support for complex input values represented by cells with relative phase shifts to account for both real and imaginary values. In our view, this implies a very efficient scheme to process environmental features with a smaller number of neurons, which is nonetheless robust to noise and input errors due to a likely redundancy of fundamental frequencies representation.

Acknowledgements

The authors thank Sucheta Chakravarty and Kenichi Kato for helpful feedback on the manuscript. Supported in part by the Natural Sciences and Engineering Research Council of Canada. The authors declare that no conflict of interest exist.

References

- Barry, C., Lever, C., Hayman, R., Hartley, T., Burton, S., O'Keefe, J., ... Burgess, N. (2006). The boundary vector cell model of place cell firing and spatial memory. *Reviews in the Neurosciences*, 17, 71-97.
- Blair, H. T., Gupta, K. C., & Zhang, K. (2008). Conversion of a phase- to a rate-coded position signal by a three-stage model of theta cells, grid cells, and place cells. *Hippocampus*, 18, 1239-1255.
- Blair, H. T., Welday, A. C., & Zhang, K. (2007). Scale-invariant memory representations emerge from moiré interference between grid fields that produce theta oscillations: A computational model. *Journal of Neuroscience*, 27(12), 3211-3229.
- Brigham, E. O. (1988). The fast fourier transform and its applications. In (chap. 3). Prentice-Hall signal processing series.
- Burgess, N. (2008). Grid cells and theta as oscillatory interference: Theory and predictions. *Hippocampus*, 18, 1157-1174.
- Burgess, N., Barry, C., & O'Keefe, J. (2007). An oscillatory interference model of grid cell firing. *Hippocampus*, 17, 801-812.
- Caplan, J. B. (2011). Grid cells and place cells as proof-of-principle for convolution-based association-memory in the medial temporal lobe. *International Conference on Memory, York, UK*.
- Field, D. J. (1987). Relations between the statistics of natural images and the response properties of cortical cells. *Optical Society of America*, 4(12), 2379-2394.
- Hafting, T., Fyhn, M., Molden, S., Moser, M.-B., & Moser, E. I. (2005). Microstructure of a spatial map in the entorhinal cortex. *Nature*, 436, 801-806.
- Hasselmo, M. E., & Brandon, M. P. (2012). A model combining oscillations and attractor dynamics for generation of grid cell firing. *Frontiers in Neural Circuits*, 6(30).
- Hasselmo, M. E., & Shay, C. F. (2014). Grid cell firing patterns may arise from feedback interaction between intrinsic rebound spiking and transverse traveling waves with

- multiple heading angles. *Frontiers in Systems Neuroscience*, 8(201).
- Hayman, R. M., & Jeffery, K. J. (2008). How heterogeneous place cell responding arises from homogeneous grids-a contextual gating hypothesis. *Hippocampus*, 18, 1301-1313.
- Hinman, J. R., Brandon, M. P., Climer, J. R., Chapman, G. W., & Hasselmo, M. E. (2016). Multiple running speed signals in medial entorhinal cortex. *Neuron*, 91(3), 666-679.
- Howard, M. W., MacDonald, C. J., Tiganj, Z., Shankar, K. H., Du, Q., Hasselmo, M. E., & Eichenbaum, H. (2014). A unified mathematical framework for coding time, space, and sequences in the hippocampal region. *Journal of Neuroscience*, 34(13), 4692-4707.
- Jeewajee, A., Barry, C., O'Keefe, J., & Burgess, N. (2008). Grid cells and theta as oscillatory interference: Electrophysiological data from freely-moving rats. *Hippocampus*, 18(12), 1175-1185.
- Kato, K., & Caplan, J. B. (2017). The brain's representations may be compatible with convolution-based memory models. *Canadian Journal of Experimental Psychology*, 71(4), 299-312.
- Krupic, J., Bauza, M., Burton, S., Barry, C., & O'Keefe, J. (2015). Grid cell symmetry is shaped by environmental geometry. *Nature*, 518(7538), 232-235.
- Krupic, J., Bauza, M., Burton, S., & O'Keefe, J. (2016). Framing the grid: effect of boundaries on grid cells and navigation. *Journal of Physiology*, 594(22), 6489-6499.
- Lever, C., Burton, S., Jeewajee, A., O'Keefe, J., & Burgess, N. (2009). Boundary vector cells in the subiculum of the hippocampal formation. *Journal of Neuroscience*, 29(31), 9771-9777.
- Li, Z.-N., & Drew, M. S. (2004). Fundamentals of multimedia. In (chap. 8). Prentice-Hall.
- Marozzi, E., Ginzberg, L. L., Alenda, A., & Jeffery, K. J. (2015). Purely translational realignment in grid cell firing patterns following nonmetric context change. *Cerebral*

- Cortex*, 25, 4619-4627.
- McCotter, M., Gosselin, F., Sowden, P., & Schyns, P. (2005). The use of visual information in natural scenes. *Visual Cognition*, 12(6), 938-953.
- Mersereau, R. M. (1979). The processing of hexagonally sampled two-dimensional signals. *Proceedings of the IEEE*, 67(6), 930-949.
- Oliva, A., & Torralba, A. (2001). Modeling the shape of the scene: A holistic representation of the spatial envelope. *International Journal of Computer Vision*, 42(3), 145-175.
- Orchard, J., Yang, H., & Ji, X. (2013). Does the entorinal cortex use the fourier transform? *Frontiers in Computational Neuroscience*, 7(179).
- Ormond, J., & McNaughton, B. L. (2015). Place field expansion after focal mec inactivations is consistent with loss of fourier components and path integrator gain reduction. *Proceedings of the National Academy of Sciences of the United States of America*, 112(13), 4116-4121.
- Pérez-Escobar, J. A., Kornienko, O., Latuske, P., Kohler, L., & Allen, K. (2016). Visual landmarks sharpen grid cell metric and confer context specificity to neurons of the medial entorhinal cortex. *eLife*, 5, e16937.
- Sargolini, F., Fyhn, M., Hafting, T., McNaughton, B. L., Witter, M. P., Moser, M.-B., & Moser, E. I. (2006). Conjunctive representation of position, direction, and velocity in entorhinal cortex. *Science*, 312(5774), 758-762.
- Snyder, W. E., Qi, H., & Sander, W. (1999). A coordinate system for hexagonal pixels. *Proceedings of the International Society for Optical Engineering*, 3661, 716-727.
- Solstad, T., Boccara, C. N., Kropff, E., Moser, M.-B., & Moser, E. I. (2008). Representation of geometric borders in the entorhinal cortex. *Science*, 322(5909), 1865-1868.
- Solstad, T., Moser, E. I., & Einevoll, G. T. (2006). From grid cells to place cells: A mathematical model. *Hippocampus*, 16, 1026-1031.
- Stachenfeld, K. L., Botvinick, M. M., & Gershman, S. J. (2017). The hippocampus as a

- predictive map. *Nature Neuroscience*, 20, 1643–1653.
- Stemmler, M., Mathis, A., & Herz, A. V. M. (2015). Connecting multiple spatial scales to decode the population activity of grid cells. *Science Advances*, 1(11).
- Stensola, H., Stensola, T., Solstad, T., Froland, K., Moser, M. B., & Moser, E. I. (2012). The entorhinal grid map is discretized. *Nature*, 492, 72–78.
- Wei, X.-X., Prentice, J., & Balasubramanian, V. (2015). A principle of economy predicts the functional architecture of grid cells. *eLife*, 4.
- Welday, A. C., Schlifer, I. G., Bloom, M. L., Zhang, K., & Blair, H. T. (2011). Cosine directional tuning of theta cell burst frequencies: Evidence for spatial coding by oscillatory interference. *Journal of Neuroscience*, 31(45), 16157–16176.

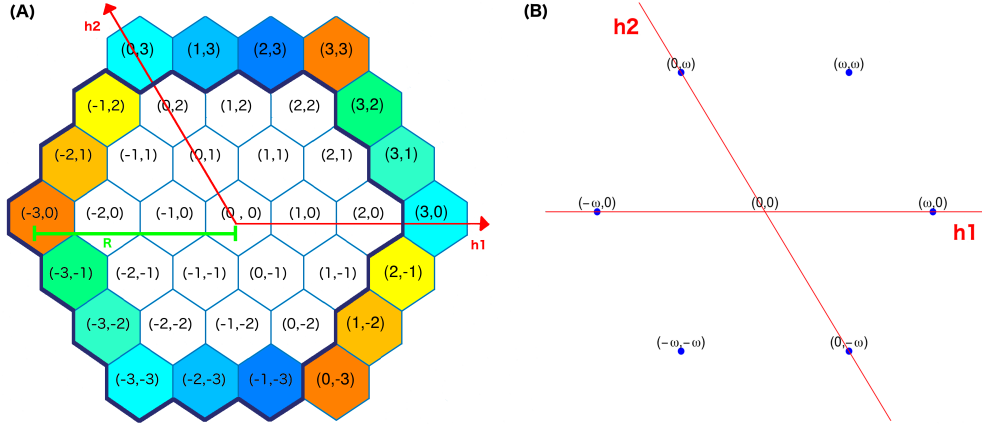


Figure 1. Illustration of the hexagonal coordinate system (A) and six frequency domain points corresponding to a single grid cell (B). \mathbf{h}_1 is the horizontal hexagonal axis and \mathbf{h}_2 is the “vertical” hexagonal axis. Each indicated coordinate is at the center of its hexagonal segment and there is R distance from $(0, 0)$ to $(-3, 0)$ in this example. A specific non-white colour for more than one hexagonal element on the boundary denotes the same element, expressing the periodic hexagonal boundary conditions. Hence, only the elements delimited by the blue perimeter are needed. (B) Six frequency points whose coordinates correspond to the coordinates of the points $\{(k_1^{(j)}, k_2^{(j)})\}_{j=1}^6$ (set of equations 9) plotted in hexagonal coordinates. ω indicates the frequency.

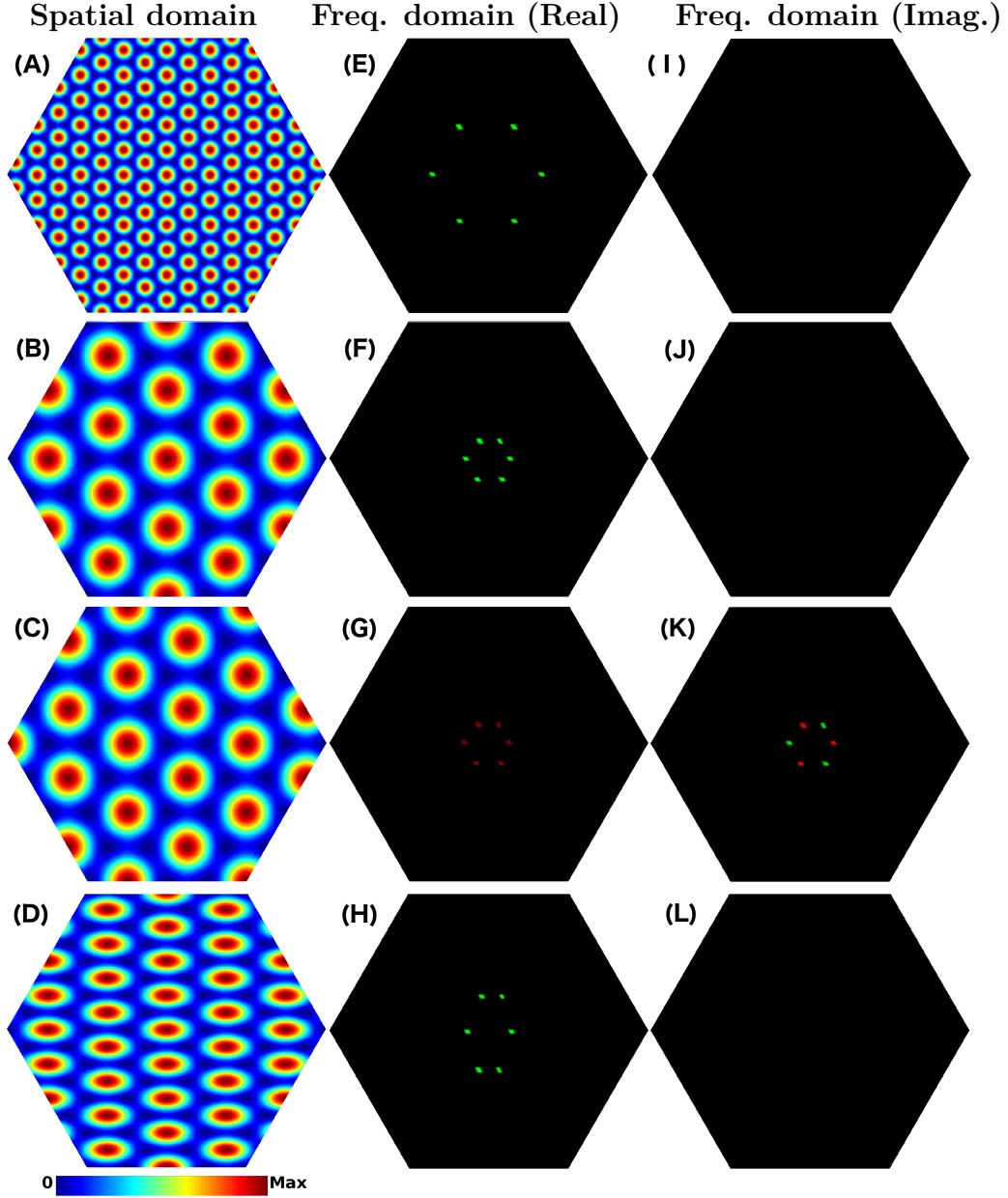


Figure 2. (A–D) grid fields generated by the inverse HDFT of the frequency domain, whose real and imaginary parts are plotted in the middle and right columns with a zoom of 400% for clarity, where low frequencies are near the center and high frequencies far away from the center. The colour bar denotes hypothetical average firing rate (arbitrary units). (A) a grid field in the spatial domain with frequency $\omega = 11$ cycles per image, which corresponds to $\sqrt{2}$ to the power of 7 rounded to the nearest integer. (B,C) two grid fields in the spatial domain with frequency $\omega = 4$ cycles per image and different phase values. Top two rows correspond to a phase with $\alpha = 0$ and $\beta = 0$. Third row: $\alpha = 64$ and $\beta = 0$ and the fourth row: $\alpha = 0$ and $\beta = 0$. (D) a regular hexagonal pattern with 4 cycles per image, that was stretched to double its frequency along the vertical direction. This corresponds to a hypothetical shrinking of the room where the rat is to half the size vertically from a baseline condition. (E–L), green indicates positive values, red negative values and black indicates zero. In all cases, $R = 128$.

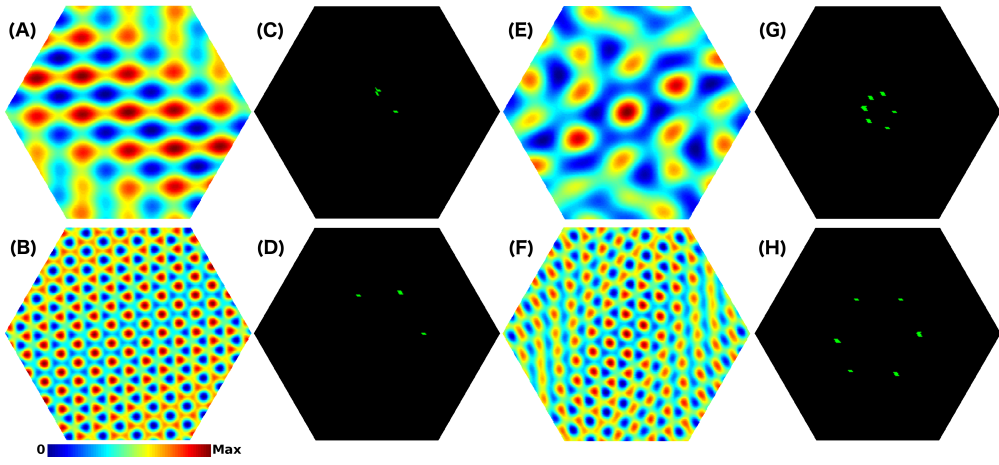


Figure 3. (A,B) grid fields with a base frequency of $\omega = 4$ and $\omega = 11$ cycles per image respectively but with noise values, drawn from a Gaussian distribution, $N(0, \sigma = 0.5)$, added to each frequency component coordinate and rounded to the nearest integer. Only three frequency components separated by approximately 60° are used. (C,D) show the real part of the frequency domain corresponding to (A,B). (E,F) show similar grid fields as in (A,B) but using six instead of three noisy frequency components. (G,H) show the real part of the frequency domain corresponding to (E,F). The colour bar denotes hypothetical average firing rate (arbitrary units). The frequency domain is shown with a zoom of 400% and in green (indicating positive values). The imaginary part is zero for all cases. In all cases $R = 128$.

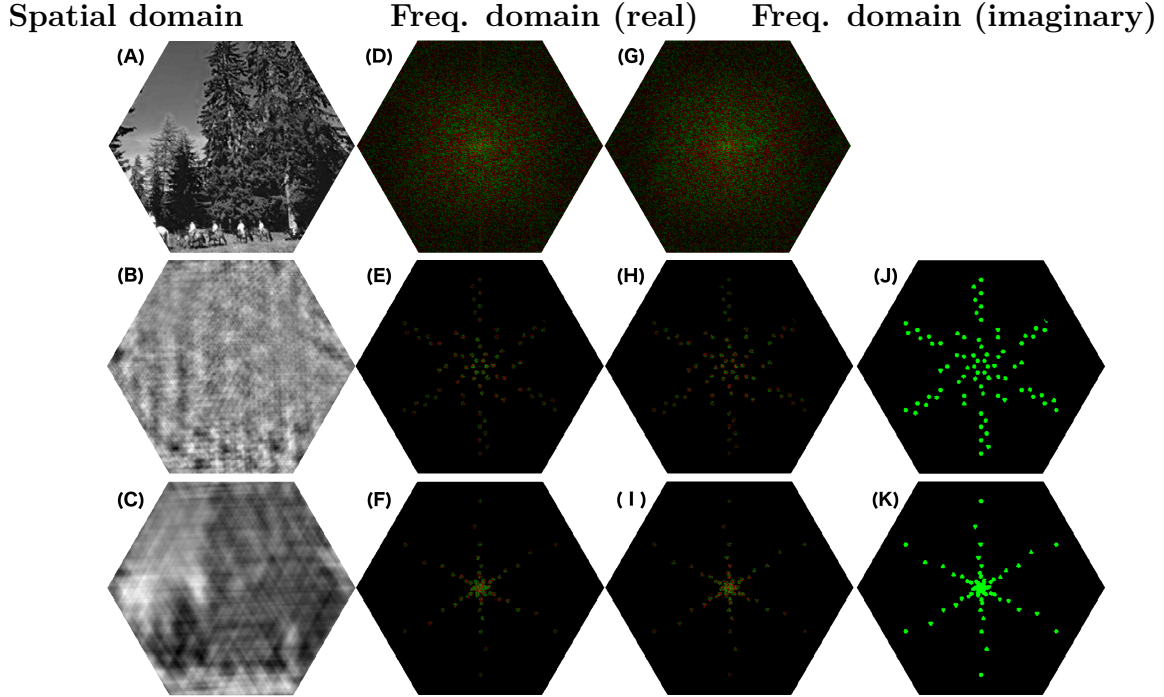


Figure 4. (A–C) an image in grayscale that corresponds to the real and imaginary frequency domain in (D–F) and (G–I), respectively. In the frequency domain, positive values are green, negative values are red and black values indicate zero. First row: original unfiltered image. Second row: LS filter with an isotropic spread in frequency of $\sqrt{5}$ cycles per image around the central frequency point of each module and 13 grid modules. Third row: ES filter with a $\sqrt{2}$ exponential base, using the same isotropic spread in frequency around the central frequency point of each module and 13 grid modules. (J,K) show the corresponding filters used in each row, for both the real and imaginary frequency domain. The orientation for each grid module is 0° , 5° , 30° or 35° , forming two orientation groups across grid modules separated by approximately 30° (Stensola et al., 2012). In all cases, 211 grid cells were used, plus the DC component.

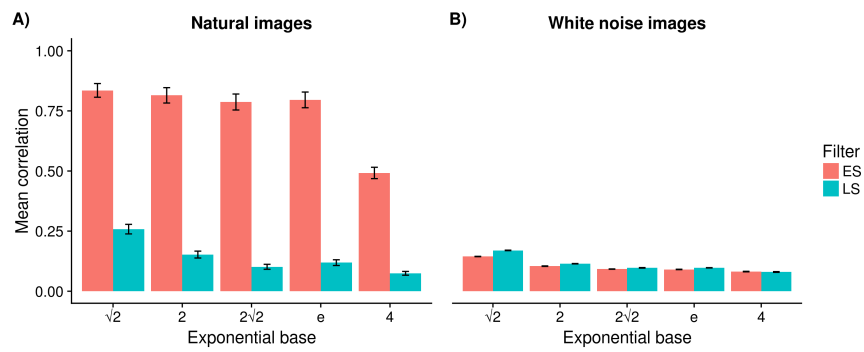


Figure 5. Mean correlation, as a measure of similarity, between the original and reconstructed image, across conditions for 100 natural (A) and 10 white-noise (B) images after filtering in the frequency domain with either exponential (ES) or linear sampling (LS) and applying the inverse HDFT. Error bars plot standard error of the mean. See Tables A and B in the Supplementary Materials respectively for the precise mean correlation values.